JGR Space Physics

RESEARCH ARTICLE
10.1029/2024JA032941

Special Collection:
Recent Discoveries in Substorm Research

Auroral and Magnetotail Dynamics During Quiet-Time STEVE and SAID

Y. Nishimura[1], B. Gallardo-Lacourt[2,3], E. F. Donovan[4], V. Angelopoulos[5], and N. Nishitani[6]

[1]Department of Electrical and Computer Engineering and Center for Space Physics, Boston University, Boston, MA, USA, [2]NASA Goddard Space Flight Center, Greenbelt, MD, USA, [3]Department of Physics, The Catholic University of America, Washington, DC, USA, [4]Department of Physics and Astronomy, University of Calgary, Calgary, AB, Canada, [5]Department of Earth, Planetary, and Space Sciences, University of California, Los Angeles, CA, USA, [6]Institute for Space Earth Environmental Research, Nagoya University, Nagoya, Japan

Key Points:

- Strong Thermal Emission Velocity Enhancement (STEVE) and subauroral ion drifts (SAID) are observed during geomagnetically quiet times when a weak auroral intensification occurs
- Quiet-time STEVE is associated with fast flows in the tail but injection is weak and temperature is low
- The quiet magnetosphere can have unique particle and current structures that drive SAID flows similar to storm times

Correspondence to:
Y. Nishimura,
toshi16@bu.edu

Citation:
Nishimura, Y., Gallardo-Lacourt, B., Donovan, E. F., Angelopoulos, V., & Nishitani, N. (2024). Auroral and magnetotail dynamics during quiet-time STEVE and SAID. *Journal of Geophysical Research: Space Physics*, *129*, e2024JA032941. https://doi.org/10.1029/2024JA032941

Received 13 JUN 2024
Accepted 27 OCT 2024

Abstract Although Strong Thermal Emission Velocity Enhancement (STEVE) and subauroral ion drifts (SAID) are often considered in the context of geomagnetically disturbed times, we found that STEVE and SAID can occur even during quiet times. Quiet-time STEVE has the same properties as substorm-time STEVE, including its purple/mauve color and occurrence near the equatorward boundary of the pre-midnight auroral oval. Quiet-time STEVE and SAID emerged during a non-substorm auroral intensification at or near the poleward boundary of the auroral oval followed by a streamer. Quiet-time STEVE only lasted a few minutes but can reappear multiple times, and its latitude was much higher than substorm-time STEVE due to the contracted auroral oval. The THEMIS satellites in the plasma sheet detected dipolarization fronts and fast flows associated with the auroral intensification, indicating that the transient energy release in the magnetotail was the source of quiet-time STEVE and SAID. Particle injection was weaker and electron temperature was lower than the events without quiet-time STEVE. The plasmapause extended beyond the geosynchronous orbit, and the ring current and tail current were weak. The interplanetary magnetic field (IMF) B_z was close to zero, while the IMF B_x was dominant. We suggest that the small energy release in the quiet magnetosphere can significantly impact the flow and field-aligned current system.

Plain Language Summary The purple/mauve-colored Strong Thermal Emission Velocity Enhancement (STEVE) emissions tend to occur at mid-latitudes during geomagnetically active times. We found that STEVE also occurs during geomagnetically quiet times. The occurrence region is much higher in latitude because the auroral oval is smaller during quiet times. Quiet-time STEVE only lasted a few minutes but can occur repetitively. Quiet-time STEVE is preceded by a weak auroral intensification and is associated with fast plasma streams in the ionosphere. The Time History of Events and Macroscale Interactions during Substorms (THEMIS) satellites in the magnetotail detected a sudden energy release, which is suggested to be the energy source for the auroral intensification and quiet-time STEVE. THEMIS also showed that the magnetosphere was very quiet and the temperature of the plasma sheet electrons was unusually low. We suggest that the sudden energy release in the quiet magnetosphere drive unexpectedly intense plasma streams and quiet-time STEVE.

1. Introduction

Strong Thermal Emission Velocity Enhancement (STEVE) is a purple/mauve-colored arc that appears near the equatorward boundary of the auroral oval, typically occurring around 60° magnetic latitude (MLAT) (MacDonald et al., 2018). STEVE is associated with intense subauroral ion drifts (SAID) during large substorms (Archer et al., 2019; Gallardo-Lacourt et al., 2018; Nishimura et al., 2019, 2020a). STEVE tends to emerge when the substorm auroral surge and streamers pass through the pre-midnight sector, indicating that fast flows and particle injections during substorms create this phenomenon. Auroral streamers often begin with a poleward boundary intensification (PBI) of the auroral oval, which is regarded as the ionospheric counterpart of magnetotail reconnection (Lyons et al., 1999). Weaker ion injection and stronger electron injection than non-STEVE injection confine the region-2 downward field-aligned currents (FACs) and to increase the conductance gradient for the formation of SAID (Nishimura et al., 2019). A recent review by Nishimura et al. (2023) describes more details on the properties of STEVE.

Although STEVE has been recognized as a phenomenon during geomagnetically disturbed times (hereinafter referred to as substorm-time STEVE), Gallardo-Lacourt et al. [submitted; attached as a related manuscript] recently showed that STEVE can also occur during quiet times. Quiet-time STEVE was detected at Yellowknife (69.4° MLAT), at a much higher latitude than substorm-time STEVE, and it has been severely underexplored. SAID are often perceived as a phenomenon during geomagnetically disturbed times, as the related FACs and precipitation are larger than during quiet times (Anderson et al., 2001). Nightside plasma flows are generally weak during quiet times, but fast and narrow plasma flows have been reported on the nightside even in quiet times, at much higher latitudes than SAID during disturbed times (Archer & Knudsen, 2018). It is not well understood how such fast flows can form during quiet times at high latitudes and how they are related to SAID.

STEVE-like emissions have also been reported at high latitudes (Dreyer et al., 2021; Whiter et al., 2021). The STEVE-like emissions have a much shorter duration (less than a minute) and appear near the poleward boundary of the auroral oval. Since quiet-time STEVE is observed near the equatorward boundary of the auroral oval, the STEVE-like emissions are different from quiet-time STEVE. Nevertheless, these works suggest that STEVE and STEVE-like emissions are not necessarily limited to disturbed conditions but could also occur in various regions and magnetic conditions.

The present study examines the auroral and magnetotail dynamics during quiet-time STEVE using simultaneous observations from all-sky imagers (ASIs) and the Time History of Events and Macroscale Interactions during Substorms (THEMIS) satellites. The first event had THEMIS at post-midnight close to the local time of auroral intensification (Section 2.1), and the second event had THEMIS at pre-midnight close to the quiet-time STEVE (Section 2.2). We also present the Super Dual Auroral Radar Network (SuperDARN) radar observations for the second event. Section 2.3 presents events without quiet-time STEVE and discusses differences between events with and without quiet-time STEVE.

2. Results

2.1. 24 February 2019 Event

Figure 1 shows solar wind and geomagnetic conditions during the event on 24 February 2019. The interplanetary magnetic field (IMF) observed by Geotail was dominated by B_x, and the IMF B_z was weakly positive (Figure 1a). The *AU*, *AL* and *SYM-H* indices were very low (Figures 1b and 1c), indicating a geomagnetically quiet time. The ground magnetic field at Rankin Inlet (72.4° MLAT and 23.8 hr MLT at 06:20 UT) remained quiet until 06:20 UT, but then showed small disturbance with $\Delta H \sim -150$ nT (Figure 1d). The enhancement in the negative *H*-component indicates an intensification of the westward electrojet in the nightside high-latitude ionosphere. Rankin Inlet is located ∼3° poleward of Fort Churchill, one of the *AE* stations. Since the *AU* and *AL* indices were small, the electrojet was located poleward of typical electrojet latitudes.

Figures 1e–1g present north-south keograms of the red, green, and blue channels from the AuroraMAX ASI at Yellowknife (69.4° MLAT and 21.5 hr MLT at 06:20 UT). AuroraMAX ASI is operated by the University of Calgary and provides colored all-sky images every 6 s. The aurora remained quiet until 06:20 UT (Figures 1e–1g). The ASI only detected a single quiet arc at ∼70° MLAT and did not show any other substantial auroral emission equatorward or poleward of the arc. Thus the auroral oval at this location was extremely thin. Even though the IMF B_z was weakly northward, the auroral arc slowly moved equatorward. It suggests that electromagnetic energy was being loaded to the magnetotail, although we do not have global imaging to accurately determine the amount of open magnetic flux. Corresponding to the ground magnetic field disturbance at 06:20 UT, an auroral intensification occurred and expanded poleward and equatorward. The auroral intensification initiated poleward of the pre-existing quiet arc. Because there was no aurora poleward of the quiet arc before 06:20 UT, the auroral intensification can be recognized as a poleward boundary intensification (PBI), which is known to occur even during quiet times (Lyons et al., 1999). Magnetotail reconnection is also known to occur during a northward IMF (Grocott et al., 2003). This was not a substorm auroral onset, because the intensification was not located equatorward of the poleward boundary of the auroral oval. The potential cause of the energy loading in the magnetotail is discussed later in this section.

This auroral intensification was associated with a peculiar emission structure near its equatorward boundary, as highlighted by the white arrow. This optical structure lasted for 5 min (06:24-06:29 UT) and was latitudinally very thin. This thin arc emerged soon after a portion of the PBI extended equatorward. While the quiet arc was mostly

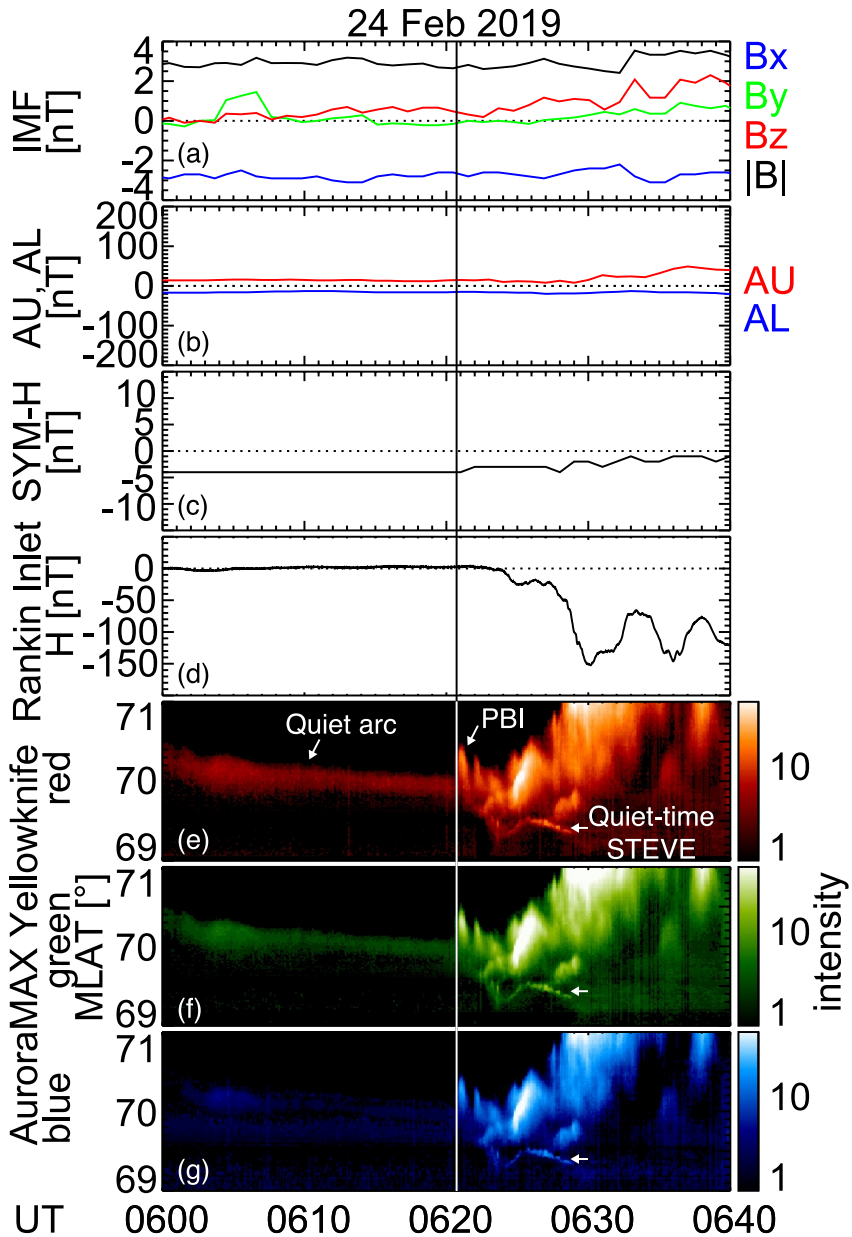

Figure 1. (a) Interplanetary magnetic field observed by Geotail (shifted to 15 R_E using the solar wind speed), (b) *AU* and *AL* indices, (c) *SYM-H* index, (d) *H*-component of the ground magnetic field at Rankin Inlet, and keograms in the (e) red, (f) green, and (g) blue channels from the AuroraMAX all-sky imager (ASI) at Yellowknife for the 24 February 2019 event. Geotail was located at (X, Y) = (25, 11) RE. The ASI intensities are arbitrarily scaled between 0 and 255.

in the red and green colors and the PBI was most dominated by the green color (note the logarithmic color scale), the thin arc had a similar intensity at all three colors. There were no other auroral structures equatorward of the thin arc, suggesting that the thin arc was located at the equatorward boundary of the auroral oval (its relation to STEVE is discussed below).

Figure 2 shows selected snapshots of (a–e) the white-light THEMIS ASIs as mosaics projected onto the map and (f–j) AuroraMAX ASI as all-sky images for this event. The aurora was quiet initially, and the faint discrete auroral arc at 70° MLAT was the only notable structure (Figures 2a and 2f). Then the auroral intensification occurred northeast of the pre-existing quiet arc (Figures 2b and 2g). Both ASIs in Figure 2b detected the auroral intensification above 70° MLAT, and there was no other auroral structure poleward of it, confirming that this intensification was a PBI. As the PBI further intensified, an auroral arc extended equatorward (Figures 2c and 2h).

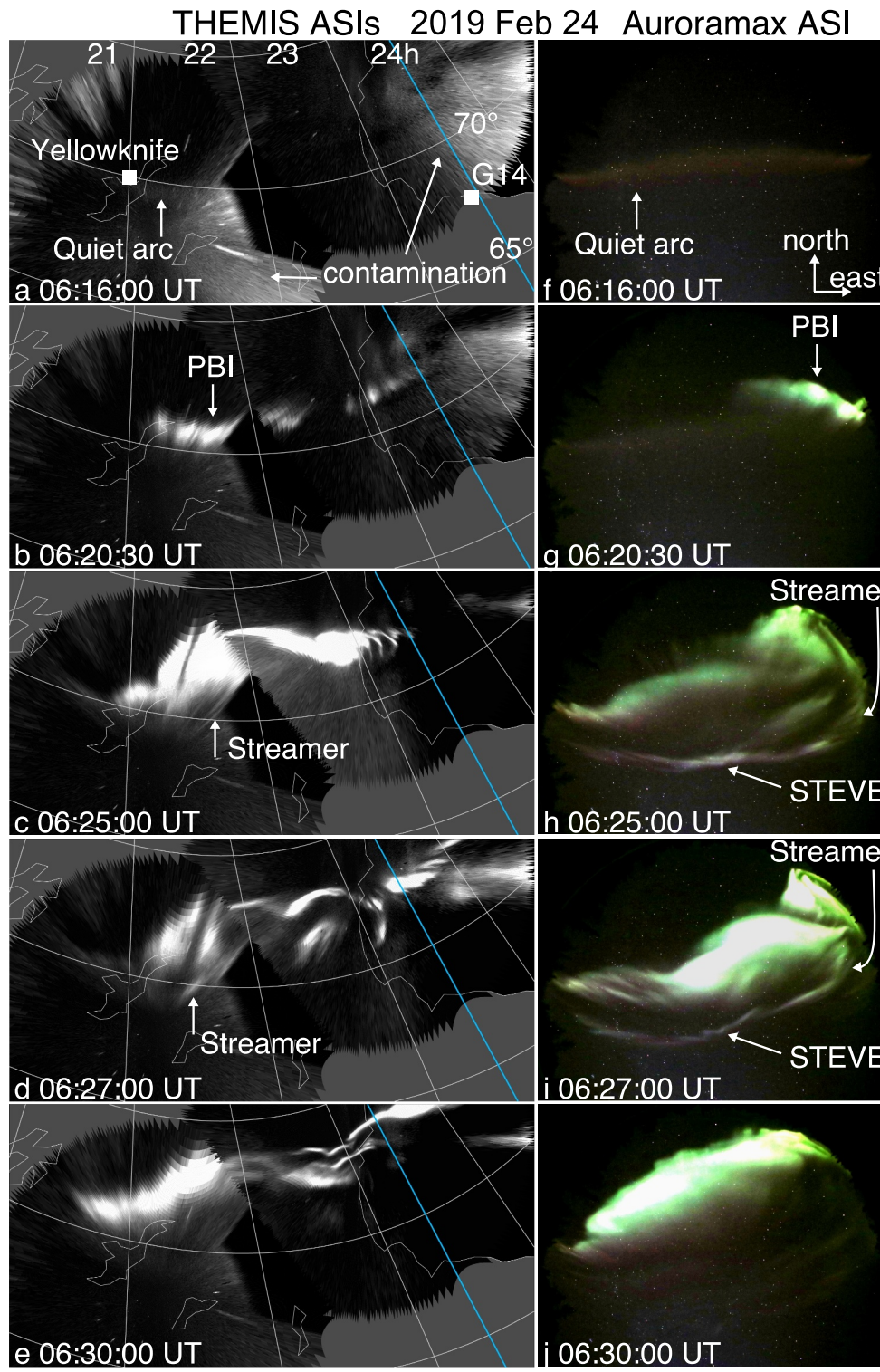

Figure 2. Selected snapshots of the all-sky imager (ASI) images from the (a–e) THEMIS ASIs at Rankin Inlet (right circle) and Fort Smith (left circle), and (f–j) AuroraMAX ASI at Yellowknife. The THEMIS ASI images are mapped to the sky at 110 km altitude. The blue line marks magnetic midnight. The Yellowknife location and magnetic footprint of GOES-14 are indicated by the white squares in Panel a. The THEMIS-D footprint is to the east of the plotted region. The AuroraMAX ASI images are presented in the all-sky format.

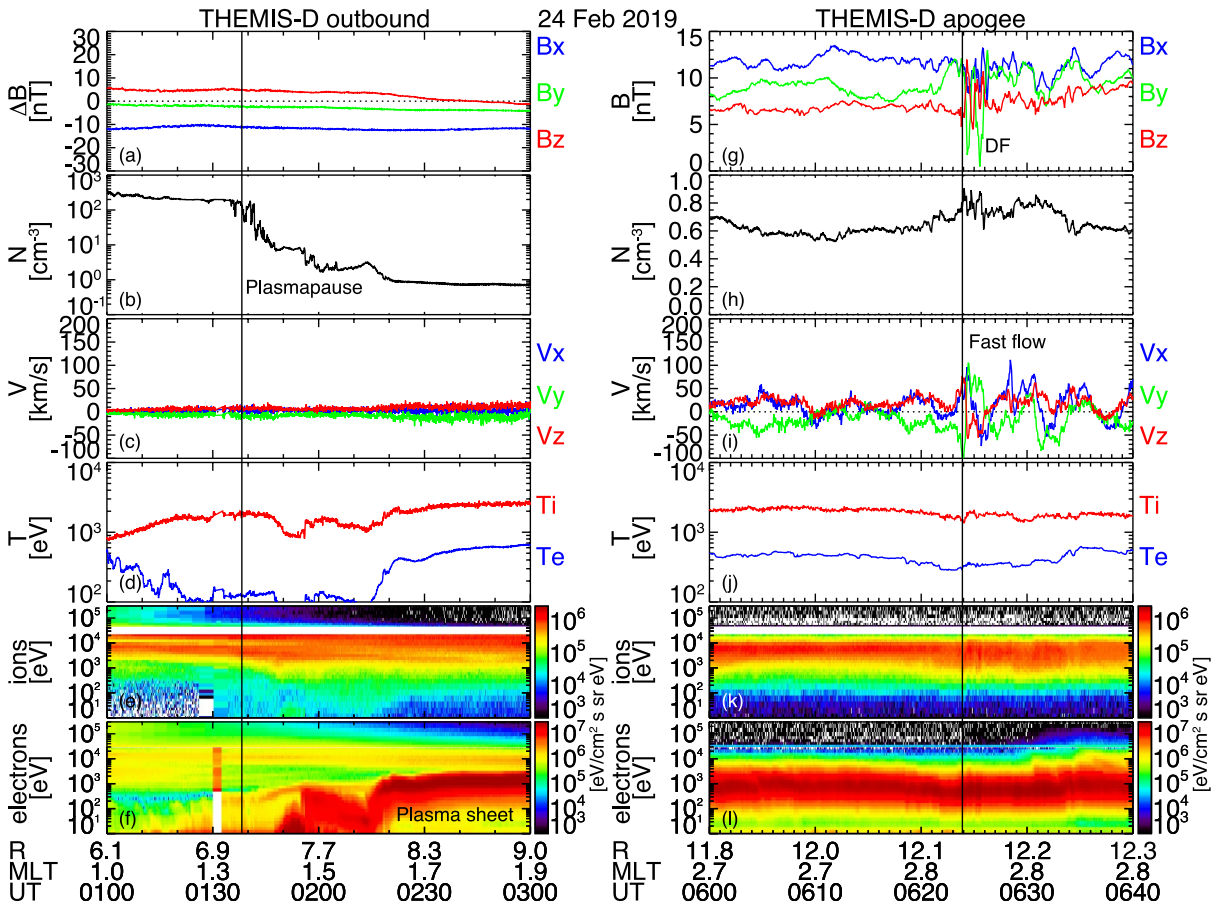

Figure 3. THEMIS-D observations at (a–f) 01:00-03:00 UT (outbound pass before Strong Thermal Emission Velocity Enhancement (STEVE)) and (g–l) 06:00-06:40 UT (during STEVE) on 24 February 2019. (a, g) Magnetic field deviation from the quiet time level, (b, h) plasma density from the spacecraft potential, (c, i) ion velocity moment, (d, j) ion and electron temperature, (e, k) ion energy flux, and (f, l) electron energy flux.

The north-south-oriented auroral structure is known as an auroral streamer (Rostoker et al., 1987). The color of the PBI and streamer was mostly green, indicating that energetic electrons created these emissions. Interestingly, the streamer was smoothly connected to an east-west oriented arc that was located equatorward of the rest of the optical emissions. The east-west-oriented portion was in the purple or mauve color. The purple/mauve arc appeared to stay connected to the green-colored streamer (Figure 2i), and then it disappeared as the streamer faded away (Figures 2e and 2j). The THEMIS ASI, however, did not detect the purple/mauve arc.

The presence of the purple/mauve arc equatorward of the auroral oval is analogous to STEVE. The occurrence after a substorm-like activity in the pre-midnight sector is also similar to the characteristics of STEVE. Although the past STEVE events have been reported at much lower latitudes (~60° MLAT) during disturbed times, the present event was observed at higher latitudes (~69.5° MLAT) during a quiet time. Because the purple/mauve arc was not visible in the THEMIS ASI, the quiet-time STEVE may be much fainter than substorm-time STEVE, and it may have been missed in previous investigations. Considering the known relation between auroral streamers and particle injections in the magnetotail [for example, Sergeev et al., 2000] (see also the THEMIS observations below), the connection between the streamer and STEVE indicates that quiet-time STEVE may be driven by particle injection. The relation to injection is in agreement with that for substorm-time STEVE (Nishimura, Yang, et al., 2020), while the connection for quiet-time STEVE can be seen more evidently because the streamer is smoothly connected to STEVE.

The THEMIS-D satellite was located in the post-midnight sector on this day. Several hours before this event, THEMIS-D was on the outbound pass and encountered the plasmapause and the earthward boundary of the electron plasma sheet outside the geosynchronous orbit (~7–8 RE, Figures 3b and 3e). This was slightly farther

outside the typical plasmapause location during quiet times (Kwon et al., 2015). ΔB was close to zero (Figure 3a), meaning that the ring current and tail current were weak and that the magnetic field configuration did not deviate largely from a typical quiet-time level. The ion velocity was low (Figure 3c), and there was no sign of SAPS or SAID at that time. These features support that the magnetosphere was very quiet.

THEMIS-D then reached near apogee (Figures 3g–3l). THEMIS-D detected a magnetic field dipolarization front (Figure 3g) and duskward flow enhancements (Figure 3i) at 06:23 UT. The ion and electron fluxes slightly increased, but there was no clear sign of particle injection. The ion and electron temperatures also did not vary substantially (Figure 3j). The electron temperature in this event was considerably low (~400 eV). The duskward flow direction indicates that the satellite was not located in the earthward-directed portion of the flow channel, but that the flow channel already turned duskward. The duskward turning of the flow channel is consistent with the duskward turning of the auroral streamer and its connection to the quiet-time STEVE in Figures 2h and 2i. These enhancements started a few minutes after the initiation of the auroral intensification in the ionosphere (06:20 UT, Figure 1), but time lag is likely because the satellite was somewhat away from the local time of the center of the auroral activity.

Figure 4a displays the IMF by Geotail starting at 4 UT. The IMF was initially northward and then became weakly southward between 04:50-06:00 UT. The southward IMF was very small and did not create any substantial auroral electrojet on the ground (Figure 4b). Figures 4c and 4d present GOES-14 observations at the geosynchronous orbit near midnight. The footprint of GOES-14 is marked in Figure 2a. GOES-14 detected a small reduction of the B_z magnetic field, indicating a thinning of the plasma sheet due to the southward IMF. It is remarkable to observe the thinning at geosynchronous orbit even with the small southward IMF. The thinning of the plasma sheet explains the equatorward motion of the quiet arc in Figures 1e–1g.

Then a small dipolarization of the magnetic field (Figure 4b) and an enhancement of energetic electron fluxes (Figure 4d) were observed at GOES-14 after 06:20 UT. Interestingly, despite the quiet conditions and small magnitude of the ground magnetic field disturbance, the disturbance in the magnetotail penetrated to the geosynchronous orbit. The ion fluxes did not change substantially (Figure 4d). The electron-dominant injection has also been seen during substorm-time STEVE, and it is suggested to be important for creating SAID (Nishimura, Yang, et al., 2020). The deep penetration of electron injection may also be a condition for creating quiet-time SAID and STEVE. This event does not have flow observations around STEVE, but the presence of quiet-time SAID is discussed in Section 2.2.

2.2. 13 April 2017 Event

Figure 5 shows the second event that occurred on 13 April 2017. This event also occurred during the quiet geomagnetic activity, where the IMF B_z was near zero, and the *AU*, *AL* and *SYM-H* indices were small. Similar to the first event, the IMF B_x was the largest component. The ground magnetic field was quiet initially and then showed a disturbance starting at 04:49 UT, although the magnitude of the disturbance was even smaller than the event in Figure 1.

The AuroraMAX ASI at Yellowknife turned on at 04:43 UT after the sunset and detected a quiet arc until 04:49 UT. The ASI image in Figure 6f shows that this was the most dominant auroral structure, but another green auroral arc was visible to the northeast. There was no other auroral emission equatorward of this arc. The blobs to the south were clouds, and the light to the west was the sunlight. A new auroral intensification occurred to the east at 04:48 UT (Figure 6g). Because it was located equatorward of the poleward-most auroral arc, this intensification was not a PBI but an auroral intensification within the auroral oval. The intensification extended westward (Figure 6h), and a green auroral arc detached from it. This may be an auroral streamer that was tilted to the east-west direction. Streamers with a large tilt from the north-south direction have often been seen (Nishimura et al., 2010). A purple/mauve emission (quiet-time STEVE) appeared equatorward of the green arc. It became more evident as the green arc faded away (Figure 6i). The sequence of southwestward-moving green arcs followed by quiet-time STEVE repeated a few times during this event (Figures 5e–5g).

The SuperDARN radar at Prince George provided line-of-sight (LOS) plasma velocity in this region. The LOS velocity was mostly away from the radar and was larger at the westward-looking beams (Figures 6a–6e), indicating that the LOS velocity was a projection of the westward flow. The velocity was moderate until 04:46 UT, and then increased to >1,000 m/s during the auroral intensification (Figure 5h). The velocity peak was located

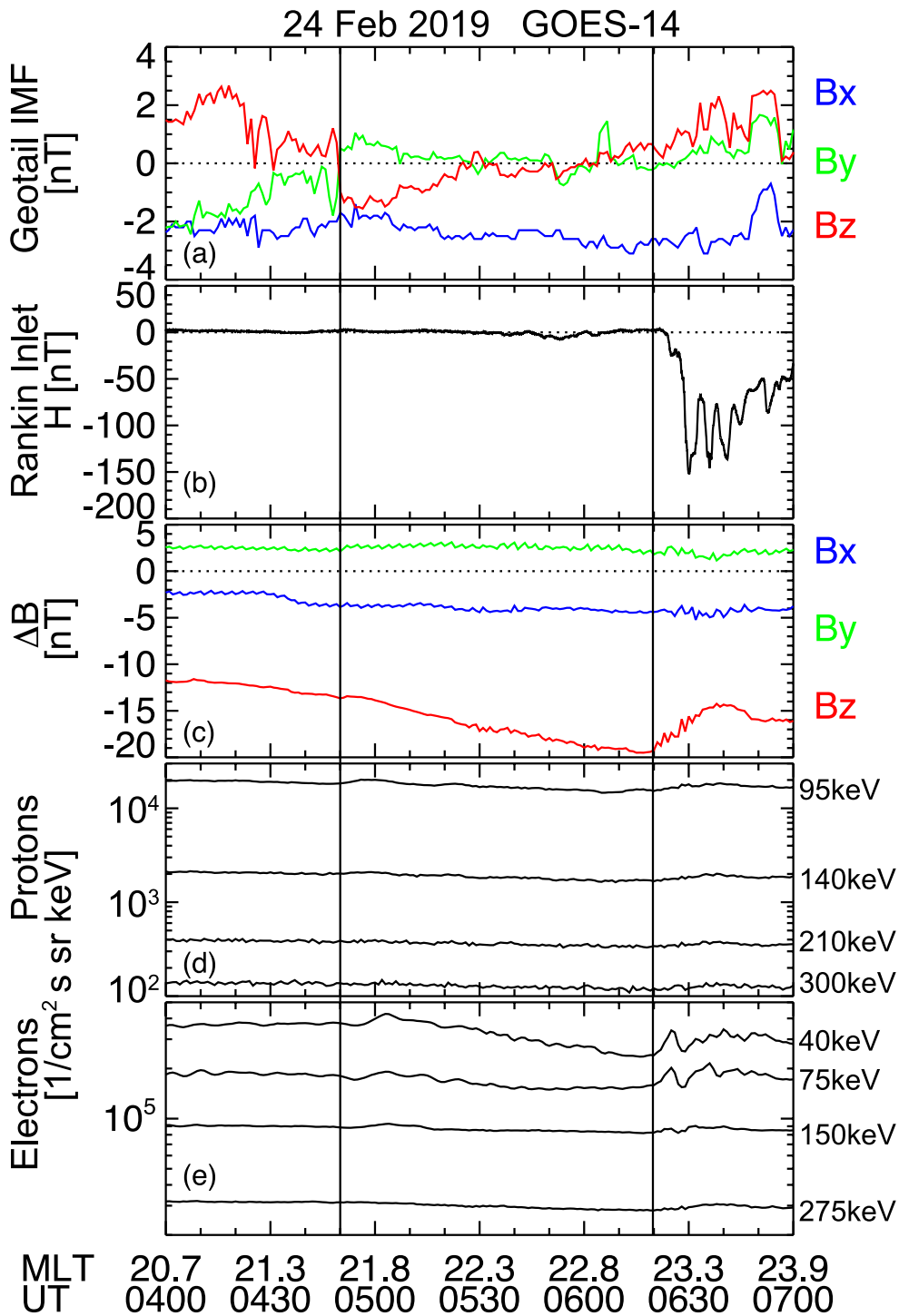

Figure 4. (a) Interplanetary magnetic field at Geotail, (b) the *H*-component of the ground magnetic field at Rankin Inlet, and GOES-14 observations of (c) the magnetic field relative to the quiet-time level, (d) proton fluxes, and (e) electron fluxes.

around the equatorward boundary of the auroral oval in the Red-line Emission Geospace Observatory (REGO) ASIs (<~69.5 ° MLAT) and occasionally formed a narrow peak reaching >1,500 m/s. The narrow velocity peak suggests the presence of SAID.

The footprints of the THEMIS D and E satellites were located within the auroral arc in the Fort Smith ASI field-of-view (FOV, Figures 6a–6e). THEMIS-D encountered the plasmapause with a plume-like density enhancement

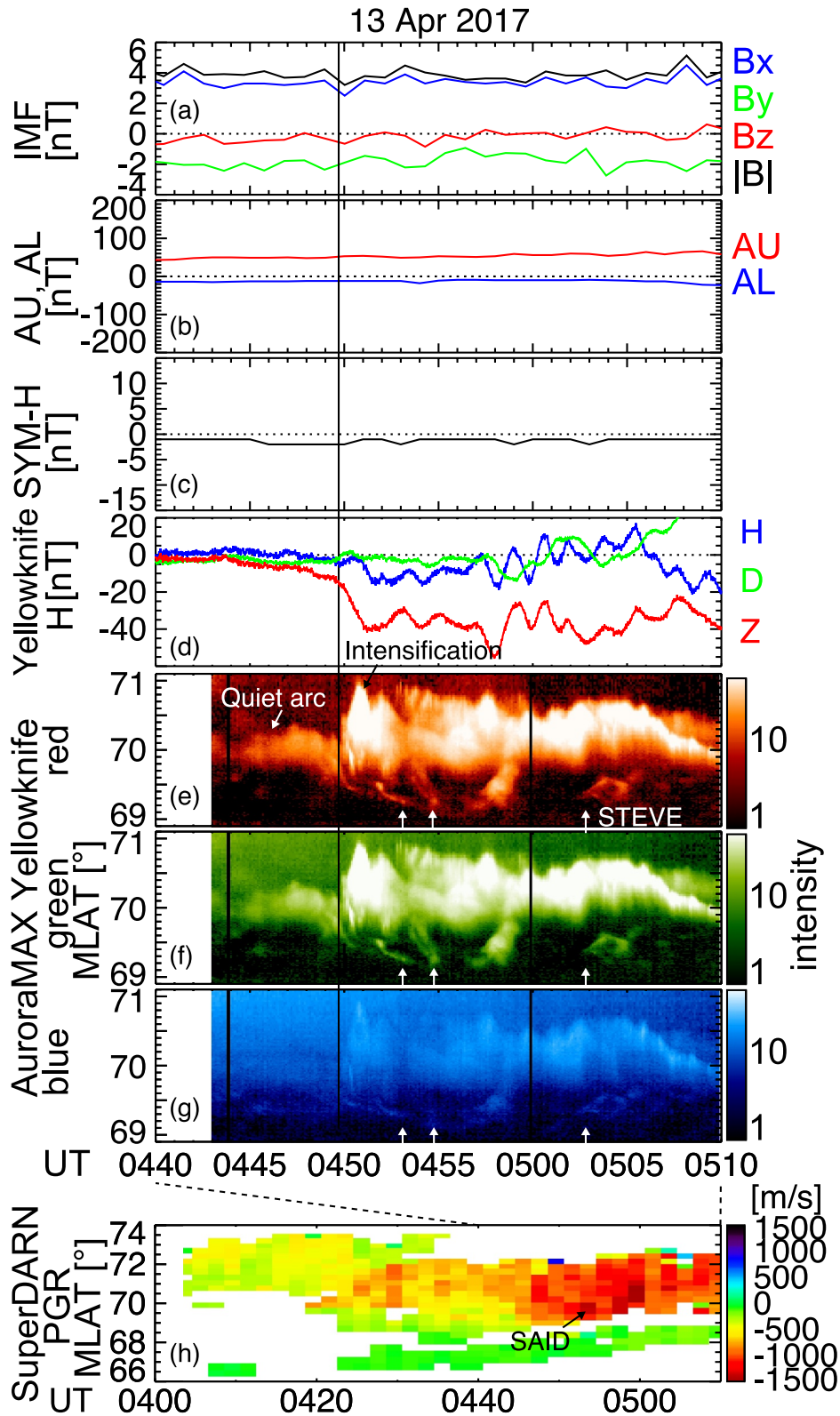

Figure 5. (a) Interplanetary magnetic field measured by Geotail (shifted to 15 R_E), (b) *AU* and *AL* indices, (c) *SYM-H* index, (d) ground magnetic field at Yellowknife, keograms in the (e) red, (f) green, and (g) blue channels from the AuroraMAX all-sky imager at Yellowknife, and (h) SuperDARN LOS velocity from the Prince George radar averaged over beam 3–6 for the 13 April 2017 event. Geotail was located at (X, Y) = (21, −17) RE.

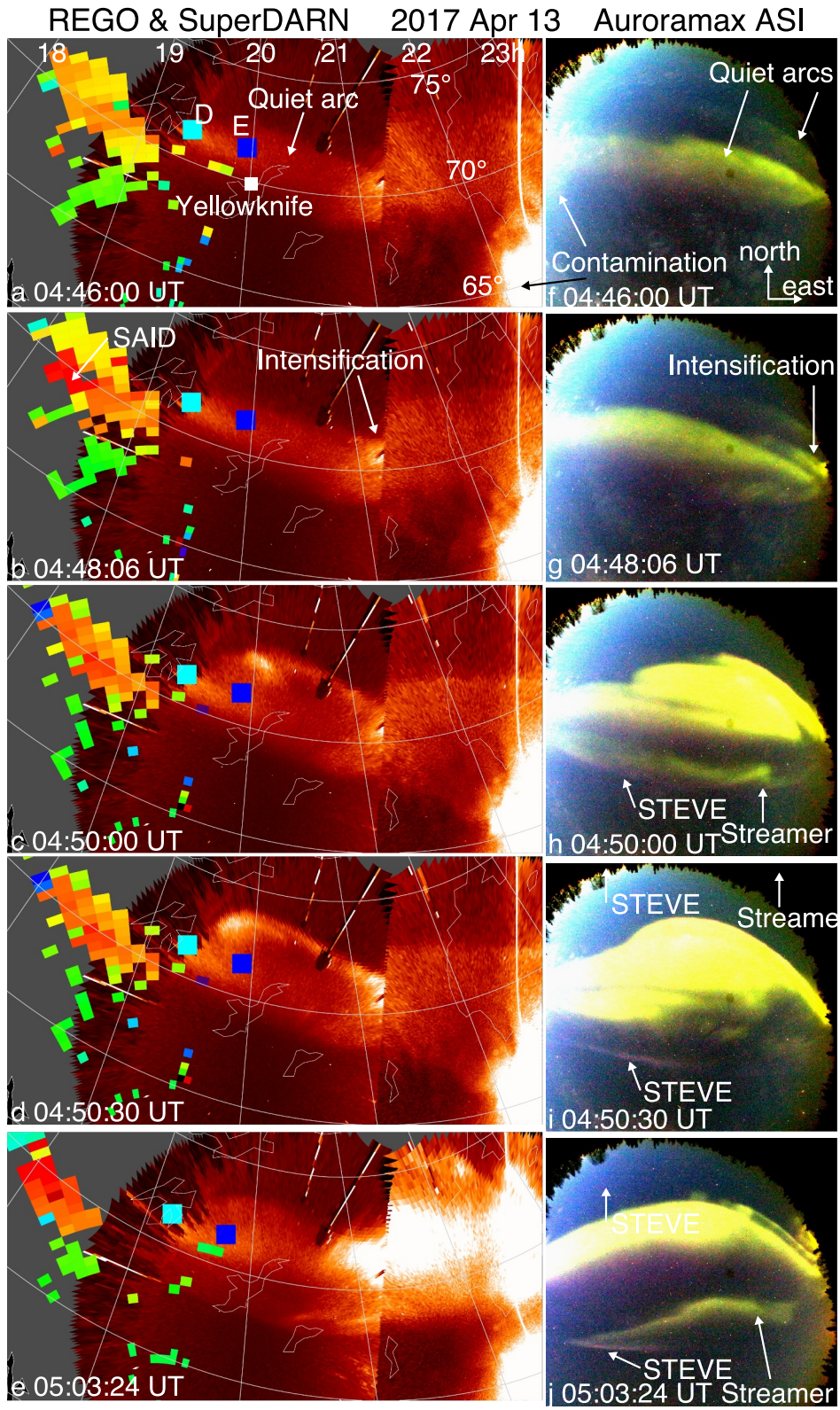

Figure 6. Selected snapshots of the all-sky imager (ASI) images from the (a–e) Red-line Emission Geospace Observatory (REGO) ASIs at Gillam and Fort Smith, and (f–j) AuroraMAX ASI at Yellowknife. The REGO ASI images are mapped to 230 km altitude. Panels (a–e) also show the SuperDARN LOS velocity from the Prince George radar in the rainbow color scale. The blue and cyan dots are the THEMIS D and E footprints. The light on the west is the sunlight.

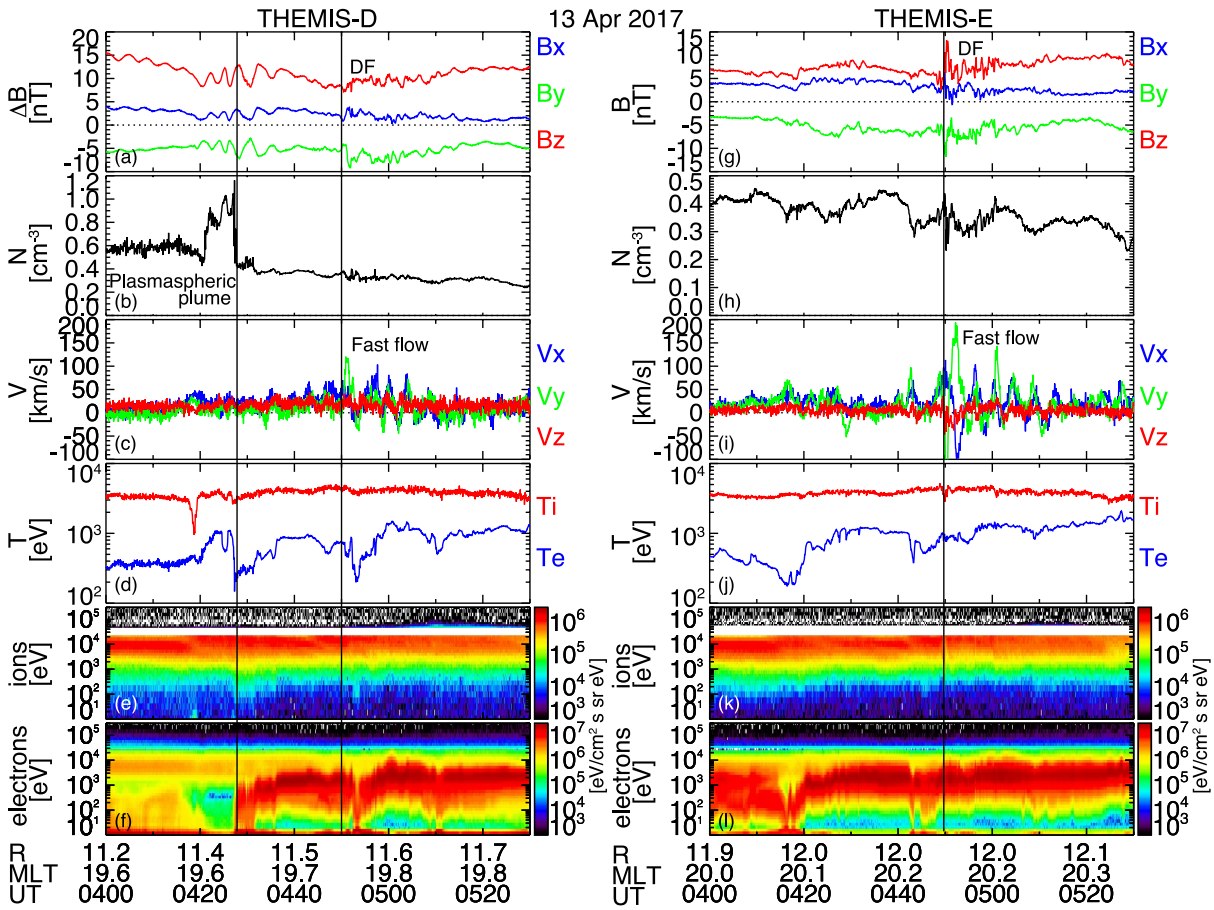

Figure 7. THEMIS-D and E observations at 4:00-5:30 UT on 13 April 2017. The format is the same as in Figure 3.

and the earthward edge of the electron plasma sheet at 11.4 R_E (Figures 7b and 7f). This plasmapause location is much farther away from the statistical plasmapause location during quiet times (Kwon et al., 2015), indicating that it was an extremely quiet time. THEMIS-E was located at 12 R_E in the electron plasma sheet throughout this time interval. THEMIS-D and E detected a magnetic field dipolarization (Figures 7a and 7g) and duskward plasma flow enhancements (Figures 7c and 7i) associated with the auroral intensification around 04:50 UT. The ion fluxes did not show substantial variations (Figures 7e and 7k). The electron fluxes at THEMIS-D dropped, and the electron energy reduced to 200 eV (Figures 7d and 7f). The electron flux at THEMIS-E did not show much variation, and the electron energy was overall around 1 keV (Figures 7j and 7l).

The IMF B_z at Geotail fluctuated near zero until ~04:20 UT and then became weakly negative (Figure 8a). The Z-component of the magnetic field at Yellowknife and GOES-13 near midnight also started to decrease around 04:20 UT. The level of magnetic field reduction was small, but it suggests energy loading to the magnetotail. Then a small increase in B_z and the electron flux was observed at GOES-13 (Figures 8c and 8e). Despite that this is a very small event, the magnetotail shows a loading-unloading cycle at geosynchronous orbit that is analogous to a substorm.

2.3. 16 February 2019 and 11 April 2017 Events (No Quiet-Time STEVE)

To compare the STEVE observations above to quiet-time data without STEVE, we present two quiet time observations on 16 February 2019 and 11 April 2017. The two events were selected from the same months and years as the events in Sections 2.1 and 2.2. We required that the magnetosphere was quiet and the THEMIS satellites were in the plasma sheet. *AU*, *AL* and *SYM-H* were small for both events. The IMF B_z was slightly negative for part of the time interval. The IMF B_x was small for the 16 February 2019 event, while it was comparable to B_z for

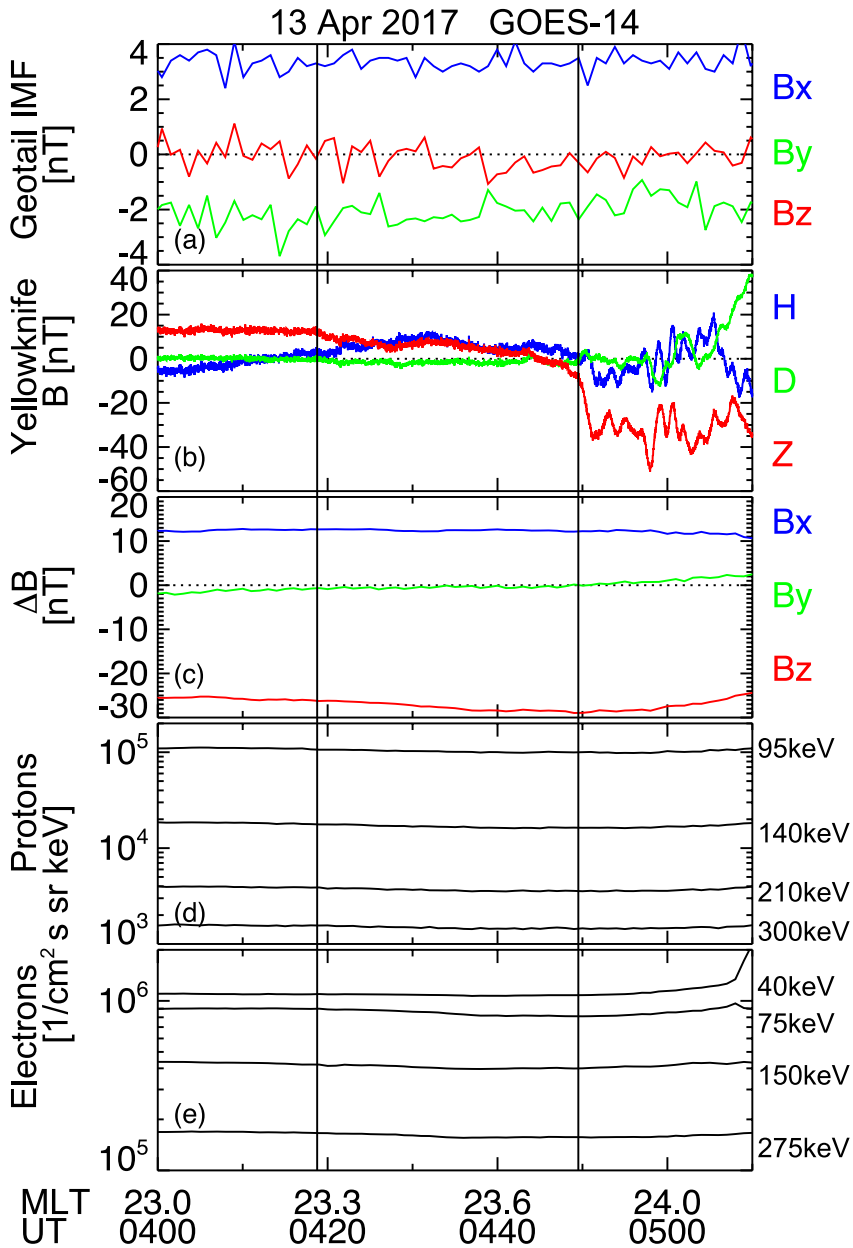

Figure 8. Same as Figure 4 but for Yellowknife magnetometer and GOES-13 observations on 13 April 2017.

the 11 April 2017 event. The ground magnetic field and aurora showed small intensifications, whose magnitudes were comparable to those in Figures 1 and 4.

Figure 10 shows snapshots of the AuroraMAX ASI images for these events. Although the moonlight blocks part of the FOV, the rest of the ASI FOV was available for viewing aurora. Similar to the earlier events, the auroral oval was quiet initially and was dominated by an auroral arc (Figures 10a and 10d). An auroral intensification occurred to the east and extended westward (Figures 10b and 10e). Some auroral structures extended equatorward during the intensification (Figures 10c and 10f), but they did not have substantial blue colored emission (Figures 7l–7n and 9e–9g). Those were mostly in the green color (Figures 10c and 10f) rather than the purple/mauve arc in the events in Sections 2.1 and 2.2.

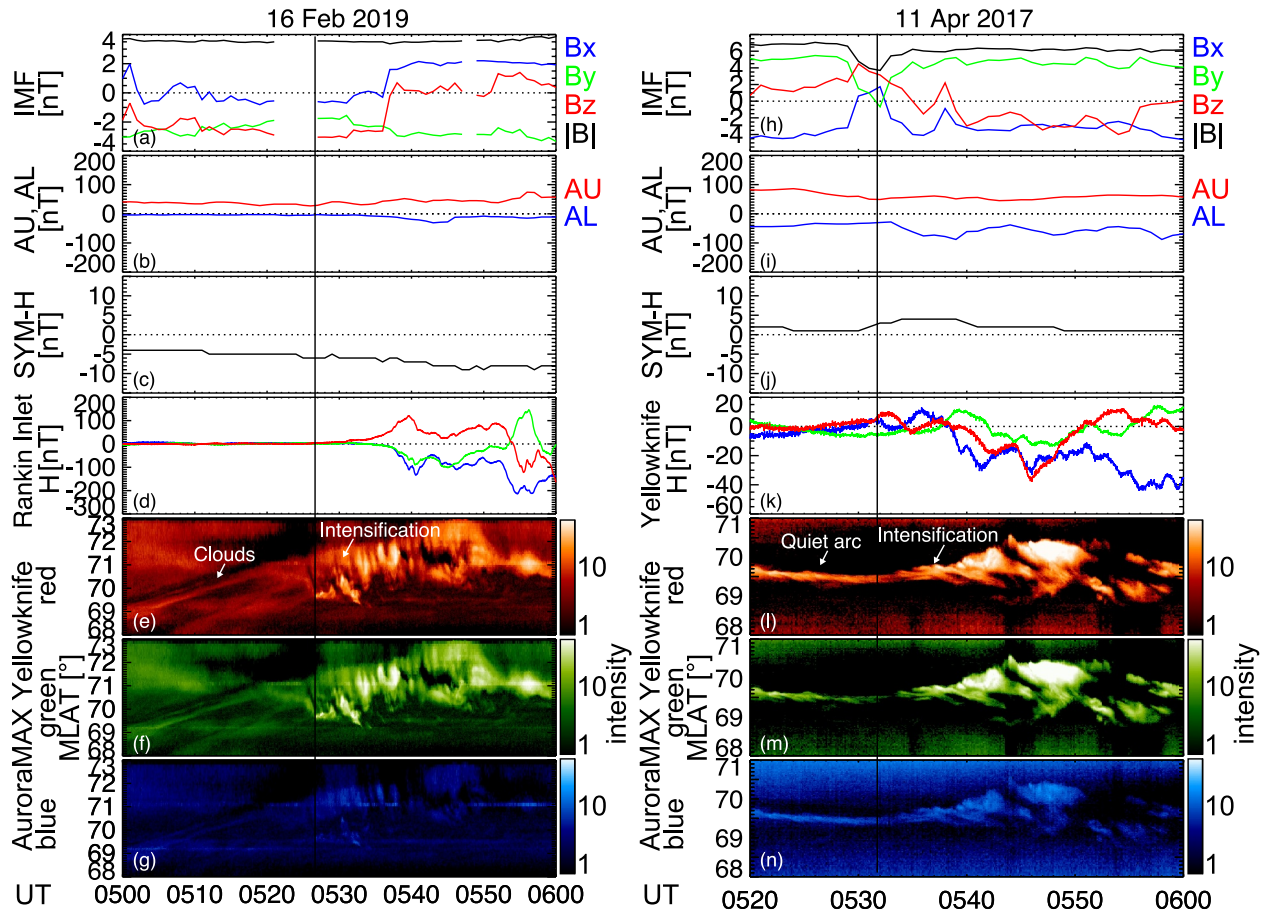

Figure 9. Two events without quiet-time Strong Thermal Emission Velocity Enhancement on (left) 16 February 2019 and (right) 11 April 2017. The format is the same as in Figure 1.

THEMIS-D was at post-midnight for the 16 February 2019 event, and THEMIS-E was at pre-midnight for the 11 April 2017 event. THEMIS-D detected multiple dipolarizations and fast flows (Figures 11a and 11c). They started earlier than the auroral intensifications in Figures 9e–9g, but it is likely because the aurora expanded from the east of Yellowknife and because the satellite was located to the east. In contrast to the event in Figure 3, the ion energy flux and temperature increased substantially (Figures 11d and 11e). The electron temperature was about twice as large (~keV). THEMIS-E observed an isolated earthward fast flow (Figure 11i) during magnetic field fluctuations (Figure 11g). In contrast to Figure 7 event, the ion and electron energy fluxes increased (Figures 11k and 11l), and the electron temperature was also elevated slightly (Figure 11j). Ion temperature variations could not be determined reliably due to the energy gap in the ion flux observations (Figure 11k).

By comparing the THEMIS observations in the events with and without quiet-time STEVE, the plasma sheet conditions have substantial differences. The events with STEVE have weaker ion injections and lower electron temperature. Weaker ion injection was also seen during substorm-time STEVE, and it has been suggested to confine the downward region-2 field-aligned currents (FAC) to a narrow region in the subauroral ionosphere (Nishimura, Yang, et al., 2020). The narrow FAC is an important condition for the formation of the SAID. The low electron temperature was not seen during substorm-time STEVE but may be a unique feature for quiet-time STEVE. The electron temperature of a few hundred eV during quiet-time STEVE is unusually low, and the low background plasma sheet temperature is known to result in low temperature in the dipolarization front (i.e., fewer energetic particles in injection) (Sergeev et al., 2015). The unique temperature conditions in the plasma sheet may alter the drift paths of plasma sheet particles from non-STEVE conditions and hence may change the FAC distributions. Although the plasma sheet density (~0.5 cm^{-3}) was not as high as that for the cold dense plasma sheet (>~1 cm^{-3}), the plasma sheet temperature decreases as cooler solar wind population enters the plasma sheet

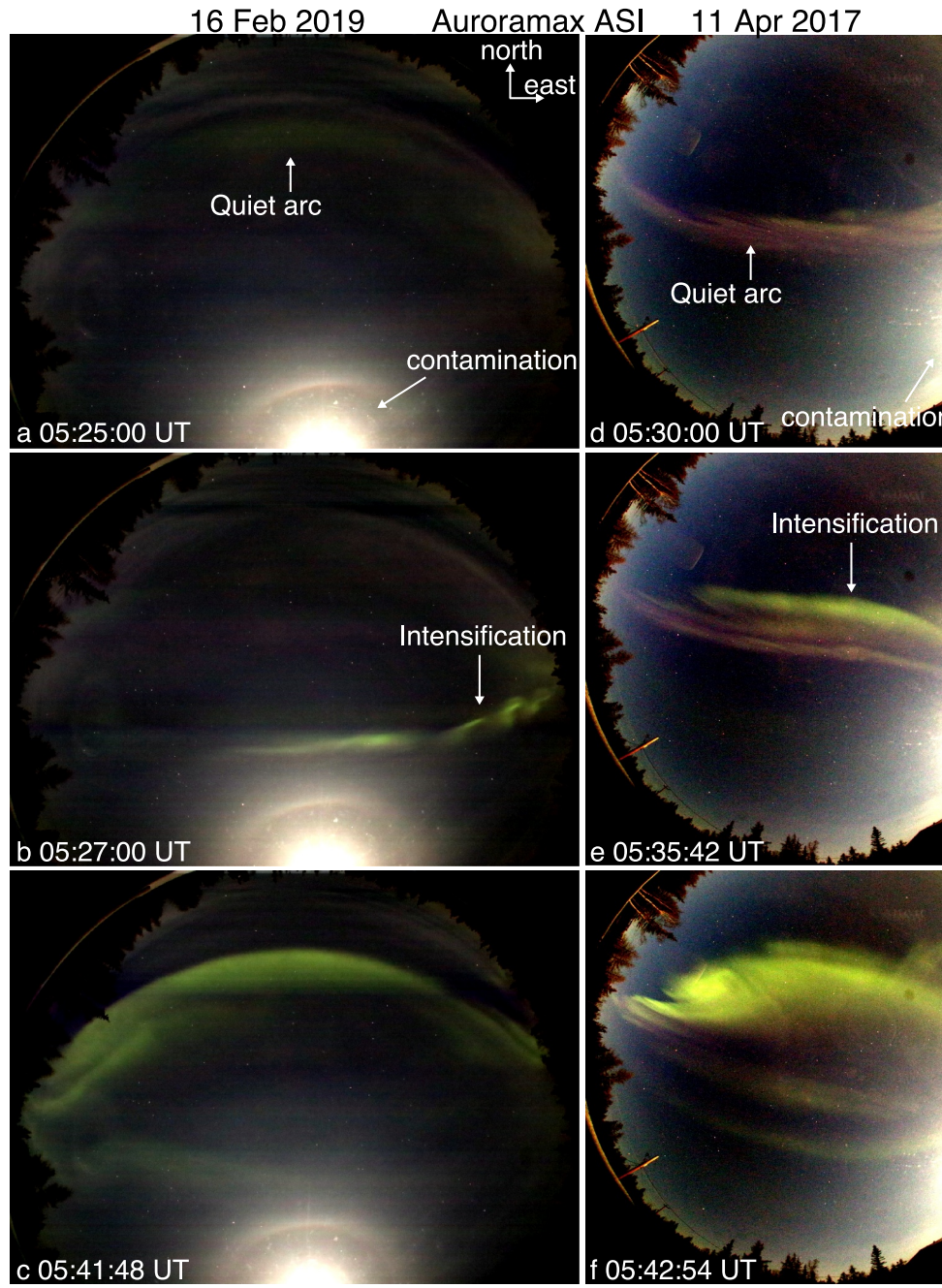

Figure 10. Selected all-sky snapshots of the AuroraMAX all-sky imager data on (left) 16 February 2019 and (right) 11 April 2017. The bright spot is the moonlight.

during quiet times (Nishino et al., 2002). The very quiet geomagnetic conditions may be important for creating the unique plasma sheet conditions for quiet-time STEVE formation.

3. Summary and Conclusion

We presented two events of STEVE emission during geomagnetically quiet periods. The IMF B_z was close to zero around the time of events, and the IMF B_x was the largest component. A weak auroral intensification occurred at or near the poleward boundary of the auroral oval. Quiet-time STEVE was identified as a distinct purple/mauve arc near the equatorward boundary of the pre-midnight auroral oval. It emerged when an auroral streamer

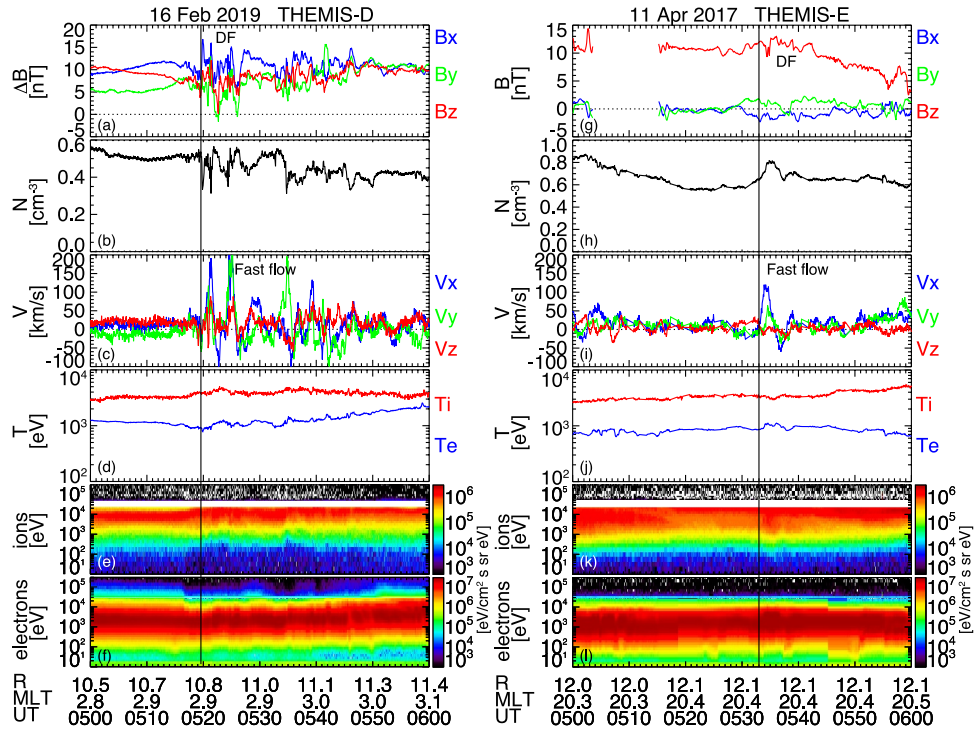

Figure 11. THEMIS observations on (left) 16 February 2019 and (right) 11 April 2017. The format is the same as in Figure 3.

extended equatorward, indicating that flow channels in the magnetotail played a role in driving quiet-time STEVE. A weak negative IMF B_z preceded quiet-time STEVE, accompanied by an increase in the tail current, indicating that a small amount of energy was loaded to the magnetotail.

Quiet-time STEVE was associated with SAID and electron-dominant injection at geosynchronous orbit. Quiet-time STEVE lasts a few minutes and can reappear multiple times during auroral intensifications. These properties are analogous to substorm-time STEVE, except that the duration of quiet-time STEVE is shorter and that they appear at higher latitudes due to the contracted auroral oval during quiet times. Quiet-time STEVE was identified in the colored ASI, but it was not visible in the white-light ASI. Quiet-time STEVE may be fainter than substorm-time STEVE.

The THEMIS satellites in the magnetotail confirmed that the auroral intensification was associated with dipolarization fronts and fast flows. However, the clear dipolarization fronts did not have strong particle injection. The electron temperature was remarkably low, reaching only a few hundred eV. The nightside plasmapause extended to unusually high L-shells (7–11 R_E), and the ring current and tail current exhibited very weak signatures. The very quiet magnetosphere and the unusual temperature conditions in the magnetotail may contribute to the formation of quiet-time STEVE by changing the drift paths of plasma sheet particles and FACs such that electron-dominant injection to the geosynchronous orbit is created and makes the width of the subauroral flow channel narrower. This hypothesis should be evaluated quantitatively through global modeling.

It is interesting to note that SAID are present even during the quiet time. SAID have often been discussed in the context of storms and substorms. The auroral and magnetospheric observations revealed that the ring current and particle injection were weak during the quiet-time STEVE events. Under those situations, generally the FACs and conductance gradient around the equatorward boundary of the auroral oval are expected to be small. However, the presence of SAID suggests that substantial FACs and conductance gradient forms despite being the quiet time. The present study focused on the events with favorable auroral and magnetospheric observations, and these events did not have low-altitude satellite or incoherent scatter radar observations during the time of interest. Evolution of FACs, precipitation and global convection should be investigated to understand how the fast plasma streams can occur during the quiet time. Also, while this study focused on the kinetic aspect as an explanation of quiet-time

STEVE, global modeling would also be needed to understand large-scale configuration of the magnetic field and convection as a potential explanation of the unusual quiet-time phenomenon.

Data Availability Statement

The THEMIS, Geotail, GOES, AuroraMAX, REGO, SuperDARN, and ground magnetometer data are available at the corresponding project websites (Angelopoulos, 2008; Candey, 2024; Chartier, 2022; Donovan, 2024; Loto'aniu, 2020). Data processing used SPEDAS-V3.1 (Angelopoulos et al., 2019).

Acknowledgments
This work was supported by NASA Grants 80NSSC20K0725, 80NSSC21K1321, 80NSSC22K0323, 80NSSC22K0749, 80NSSC23M0193, 80NSSC23K0410, 80NSSC24K1103, and 80NSSC24K1862, NSF Grants AGS-1907698 and AGS-2100975, and AFOSR Grants FA9550-23-1-0614 and FA9550-23-1-0634. THEMIS is supported by NASA NAS5-02099 and Canada Foundation for Innovation. We thank ISSI/ISSJ-BJ through ISSI International Team projects Auroral Research Coordination: Towards Internationalised Citizen Science (ARCTICS), Multi-Scale Magnetosphere-Ionosphere-Thermosphere Interaction, and Magnetotail Dipolarizations: Archimedes Force or Ideal Collapse?

References

Anderson, P. C., Carpenter, D. L., Tsuruda, K., Mukai, T., & Rich, F. J. (2001). Multisatellite observations of rapid subauroral ion drifts (SAID). *Journal of Geophysical Research*, *106*(A12), 29585–29599. https://doi.org/10.1029/2001JA000128

Angelopoulos, V. (2008). THEMIS mission website (THEMIS satellites, ASI and ground magnetometers) [Dataset]. University of California. Retrieved from https://themis.ssl.berkeley.edu/themisdata/thd/l2/, https://themis.ssl.berkeley.edu/themisdata/the/l2/, https://themis.ssl.berkeley.edu/themisdata/thg/l2/mag/ and https://themis.ssl.berkeley.edu/themisdata/thg/l1/asi/

Angelopoulos, V., Cruse, P., Nishimura, Y., Grimes, E. W., Hatzigeorgiu, N., King, D. A., THEMIS group, et al. (2019). The Space Physics Environment Data Analysis System (SPEDAS). *Space Science Reviews*, *215*(1), 9. https://doi.org/10.1007/s11214-018-0576-4

Archer, W. E., Gallardo-Lacourt, B., Perry, G. W., St.-Maurice, J.-P., Buchert, S. C., & Donovan, E. F. (2019). Steve: The optical signature of intense subauroral ion drifts. *Geophysical Research Letters*, *46*(12), 6279–6286. https://doi.org/10.1029/2019gl082687

Archer, W. E., & Knudsen, D. J. (2018). Distinguishing subauroral ion drifts from Birkeland current boundary flows. *Journal of Geophysical Research: Space Physics*, *123*(1), 819–826. https://doi.org/10.1002/2017ja024577

Candey, R. (2024). Space physics data facility (Geotail) [Dataset]. Goddard Space Flight Center. Retrieved from https://cdaweb.gsfc.nasa.gov/pub/data/geotail/

Chartier, A. (2022). SuperDARN FITACF v2.5 and v3.0 data [Dataset]. Johns Hopkins University. Retrieved from https://superdarn.jhuapl.edu/download

Donovan, E. F. (2024). UCalgary space remote sensing open data platform (AuroraMAX, REGO) [Dataset]. University of Calgary. Retrieved from https://data.phys.ucalgary.ca/sort_by_instrument/all_sky_camera/GO-Canada_REGO/andhttps://data.phys.ucalgary.ca/sort_by_instrument/all_sky_camera/AuroraMAX_SLR/

Dreyer, J., Partamies, N., Whiter, D., Ellingsen, P. G., Baddeley, L., & Buchert, S. C. (2021). Characteristics of fragmented aurora-like emissions (FAEs) observed on Svalbard. *Annals of Geophysics*, *39*(2), 277–288. https://doi.org/10.5194/angeo-39-277-2021

Gallardo-Lacourt, B., Nishimura, Y., Donovan, E., Gillies, D. M., Perry, G. W., Archer, W. E., et al. (2018). A statistical analysis of STEVE. *Journal of Geophysical Research: Space Physics*, *123*(11), 9893–9905. https://doi.org/10.1029/2018ja025368

Grocott, A., Cowley, S. W. H., & Sigwarth, J. B. (2003). Ionospheric flow during extended intervals of northward but BY-dominated IMF. *Annales Geophysicae*, *21*(2), 509–538. https://doi.org/10.5194/angeo-21-509-2003

Kwon, H.-J., Kim, K.-H., Jee, G., Park, J.-S., Jin, H., & Nishimura, Y. (2015). Plasmapause location under quiet geomagnetic conditions (Kp ≤ 1): THEMIS observations. *Geophysical Research Letters*, *42*(18), 7303–7310. https://doi.org/10.1002/2015GL066090

Loto'aniu, P. (2020). GOES-R space weather [Dataset]. National Oceanic and Atmospheric Administration. Retrieved from https://www.ngdc.noaa.gov/stp/satellite/goes-r.html

Lyons, L. R., Nagai, T., Blanchard, G. T., Samson, J. C., Yamamoto, T., Mukai, T., et al. (1999). Association between Geotail plasma flows and auroral poleward boundary intensifications observed by CANOPUS photometers. *Journal of Geophysical Research*, *104*(A3), 4485–4500. https://doi.org/10.1029/1998JA900140

MacDonald, E. A., Donovan, E. F., Nishimura, Y., Case, N. A., Gillies, D. M., Gallardo-Lacourt, B., et al. (2018). New science in plain sight: Citizen scientists lead to discovery of optical structure in the upper atmosphere. *Science Advances*, *4*(3), eaaq0030. https://doi.org/10.1126/sciadv.aaq0030

Nishimura, Y., Donovan, E. F., Angelopoulos, V., & Nishitani, N. (2020a). Dynamics of auroral precipitation boundaries associated with STEVE and SAID. *Journal of Geophysical Research: Space Physics*, *125*(8), e2020JA028067. https://doi.org/10.1029/2020ja028067

Nishimura, Y., Dyer, A., Kangas, L., Donovan, E., & Angelopoulos, V. (2023). Unsolved problems in Strong thermal Emission Velocity Enhancement (STEVE) and Picket Fence. *Frontiers in Astronomy and Space Sciences*, *10*. https://doi.org/10.3389/fspas.2023.1087974

Nishimura, Y., Gallardo-Lacourt, B., Zou, Y., Mishin, E., Knudsen, D. J., Donovan, E. F., et al. (2019). Magnetospheric signatures of STEVE: Implications for the magnetospheric energy source and interhemispheric conjugacy. *Geophysical Research Letters*, *46*(11), 5637–5644. https://doi.org/10.1029/2019gl082460

Nishimura, Y., Lyons, L., Zou, S., Angelopoulos, V., & Mende, S. (2010). Substorm triggering by new plasma intrusion: THEMIS all-sky imager observations. *Journal of Geophysical Research*, *115*(A7), A07222. https://doi.org/10.1029/2009JA015166

Nishimura, Y., Yang, J., Weygand, J. M., Wang, W., Kosar, B., Donovan, E. F., et al. (2020). Magnetospheric conditions for STEVE and SAID: Particle injection, substorm surge, and field-aligned currents. *Journal of Geophysical Research: Space Physics*, *125*(8), e2020JA027782. https://doi.org/10.1029/2020ja027782

Nishino, M. N., Terasawa, T., & Hoshino, M. (2002). Increase of the tail plasma content during the northward interplanetary magnetic field intervals: Case studies. *Journal of Geophysical Research*, *107*(A9), 1261. https://doi.org/10.1029/2002JA009268

Rostoker, G., Lui, A. T. Y., Anger, C. D., & Murphree, J. S. (1987). North-south structures in the midnight sector auroras as viewed by the viking imager. *Geophysical Research Letters*, *14*(4), 407–410. https://doi.org/10.1029/GL014i004p00407

Sergeev, V., Sauvaud, J. A., Popescu, D., Kovrazhkin, R. A., Liou, K., Newell, P. T., et al. (2000). Multiple-spacecraft observation of a narrow transient plasma jet in the Earth's plasma sheet. *Geophysical Research Letters*, *27*(6), 851–854. https://doi.org/10.1029/1999GL010729

Sergeev, V. A., Dmitrieva, N. P., Stepanov, N. A., Sormakov, D. A., Angelopoulos, V., & Runov, A. V. (2015). On the plasma sheet dependence on solar wind and substorms and its role in magnetosphere-ionosphere coupling. *Earth Planets and Space*, *67*(1), 133. https://doi.org/10.1186/s40623-015-0296-x

Whiter, D. K., Sundberg, H., Lanchester, B. S., Dreyer, J., Partamies, N., Ivchenko, N., et al. (2021). Fine-scale dynamics of fragmented aurora-like emissions. *Annals of Geophysics*, *39*(6), 975–989. https://doi.org/10.5194/angeo-39-975-2021